Journal of Wasit for Science and Medicine 2026: 19, (3), 93-106

A Computational Study of Doxorubicin Transport in a Tumor Microenvironment: Influence of Interstitial Fluid Pressure

Zeina Salman

Department of Physics, College of Science, Wasit University, Al Kut, Wasit, Iraq

zsalman@uowasit.edu.iq

Abstract

Interstitial fluid pressure (IFP) increases in solid tumors, which drives the convective flow away from the tumor center, preventing penetration of chemotherapy. A convection-diffusion-reaction model coupled with the Darcy-Starling equation was used to model the motion of Doxorubicin in a 1 cm radius tumor. The IFP was analytically obtained based on the modified spherical Bessel equation, and checked numerically, with a maximum residual error of less than 10^{-8} Pa. Results show an outward flow velocity up to 43.75 nm s^{-1} within a peripheral shell of 0.31 mm accompanied by tumor core IFP of 5 mmHg. At t = 3 h, drug concentrations were 19% of plasma peak with a steady rim-to-core gradient. A parametric study varying vascular pressure (600-3000 Pa) verified that bulk drug supply is regulated by transvascular supply while IFP regulates the peripheral concentration gradient. The results support the vascular normalization strategy to improve intratumoral drug delivery.

Keywords: drug delivery; convection-diffusion; vascular normalization.

1. Introduction

One of the most challenging issues with oncology is delivering chemotherapy appropriately to solid tumors. Through decades of pharmaceutical research, many of the systemically delivered chemotherapeutic agents fail to sufficiently transport therapeutic concentrations into the interior of the tumor [1, 2]. This is not only because of pharmacokinetic limitations and inadequate drug chemistry, but also because the abnormal physical microenvironment of solid tumors imposes structural obstacles to

drug delivery that operate regardless of drug design [3]. Of these, the increase of the interstitial fluid pressure (IFP) is probably the most significant and most well defined. The interstitial pressure of normal tissues is a little below atmospheric (around -2 to 0 mmHg) which ensures a hydrostatic gradient between the vasculature and the interstitium which facilitates convective movement of drugs [4]. However, in solid tumors a cluster of structural abnormalities collectively eliminates this gradient. These are strongly permeable and disorganized neovascular networks, an almost complete lack of the functional intratumoral lymphatics, high interstitial matrix density and solid mechanical stress [5, 6]. Combined, these qualities result in tumor IFP readings of 10-40 mmHg in clinical measurements [6, 7], and there are some that are as high as 94 mmHg [8]. High IFP produces an outward convective flux across the tumor border which actively counteracts the inward drug delivery, especially that of macromolecules and nanoparticles the transport of which is dominated by convection [3].

Essential progress in quantitative modeling of fluid flow and drug transport in tumors was initiated by a series of studies by Baxter and Jain [9, 10] on a new paradigm of modeling of tumor interstitial fluid behavior in the Darcy–Starling framework. Their results proved that high IFP is the result of balancing between interstitial pressure and effective vascular pressure in the absence of lymphatic drainage and that this balance forms a spatially flat profile of IFP at the center of the tumor with a steep decline at the tumor periphery. This framework has been generalized to heterogeneous tumor geometries [11], nanomedicine transport [12] and the impact of anti-angiogenic therapy on drug penetration [13] through subsequent computational works. More recently analytical and idealized models have been superseded by patient specific models based on medical imaging [14], but they have an important role in parameter sensitivity analysis and mechanistic understanding.

Doxorubicin is an anthracycline antibiotic that is commonly used and has proven to be effective with breast, ovarian, hepatocellular, and bladder malignancies [15]. It is transported in tumor tissue by a low diffusivity with D*eff* = 2.4×10^{-12} m^2 s^{-1} [16] and is no longer transported by diffusion along the

boundaries, but solely by transvascular supply instead, thus it has become an important factor affecting its intratumoral distribution. Whereas the interplay between the magnitude of IFP, outward convective velocity, and diffusion of Doxorubicin has been experimentally studied over several decades, the interplay between the three parameters in a parametric computational model with an analytical validation is not well-mapped.

In the current research, we construct, analytically solve, and numerically validate a 1D axisymmetric transport model of Doxorubicin diffusion in a tumor, which is spherical. The objectives of this study are: (i) finding an analytical solution of the steady-state spherically coordinated IFP distribution; (ii) verifying the analytical solution with a numerical boundary-value solver; (iii) performing a systematic parametric study of the effect of vascular pressure on drug penetration depth and intratumoral concentration gradients. Findings are discussed with regard to IFP lowering via vascular normalization [17] as a clinically implementable concept to enhance chemotherapy efficacy. Figure 1 shows the model geometry.

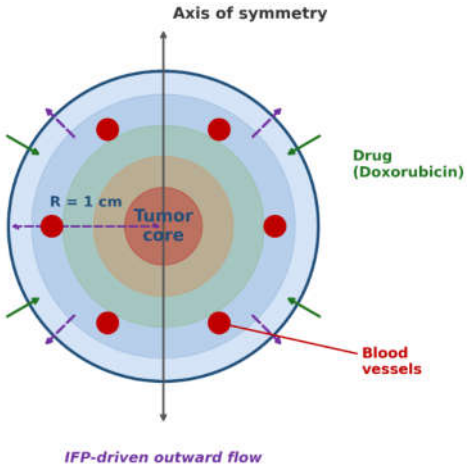

Figure 1 Cross sectional view of the 2D axisymmetric tumor model. Blood vessels throughout the tumor parenchyma are shown as red filled circles. The inward transport of Doxorubicin drug is shown by green arrows. IFP is shown in purple dashed arrows and is mainly directed outwards near the tumor rim. R = 1 cm.

2. Mathematical Model

2.1 Model Geometry and Assumptions

The tumor is assumed to be a uniform sphere with a radius of R = 1 cm. With axisymmetry, all of the governing equations become one-dimensional in space - the radial direction r ranging from 0 to R. It is a standard geometry used in the tumor transport literature and both an analytical and efficient numerical solution can be obtained with this geometry [9, 10, 18]. The assumptions made include the following: (i) Tumor is homogeneous with spatially homogeneous vascular and transport parameters; (ii) cellular drug uptake will

not be explicitly modelled but lumped into the rate constant kel; (iii) the IFP is in steady state before drug administration is started; (iv) plasma drug concentration is described by a first-order pharmacokinetic model. These assumptions can be related to the initial Baxter-Jain model [9, 10] and are suitable in the context of this research.

2.2 Interstitial Fluid Pressure

The physical laws that control the fluid flow through the interstitium are the law of Darcy and exchange of fluid across the vessel wall occurs with the help of Starling equation. Adding these to the mass conservation results in:

$$\mathbf{Ki\ \nabla^2 Pi = Lp(S/V)[(Pi - Pv) + \sigma f(\pi v - \pi i)]} \quad (1)$$

Ki is the interstitial hydraulic conductivity ($m^2\ Pa^{-1}\ s^{-1}$), Lp is the vascular wall hydraulic conductivity ($Pa^{-1}\ s^{-1}$), S/V is the vascular surface area per unit volume (m^{-1}), Pv is vascular pressure (Pa) and πv and πi are the vascular and interstitial osmotic pressures respectively. In terms of α = Lp(S/V)/Ki (m^{-2}) and the effective vascular driving pressure the spherically symmetric form of this equation is:

$$\mathbf{d^2Pi/dr^2 + (2/r)(dPi/dr) = \alpha(Pi - Pe)} \quad (2)$$

This becomes the modified spherical Bessel equation of zeroth order. The physically regular solution (regular at r=0) is:

$$\mathbf{Pi(r) = Pe + (Pi,b - Pe)(R/r) \cdot \sinh(\sqrt{\alpha}\, r) / \sinh(\sqrt{\alpha}\, R)} \quad (3)$$

where Pi,b is the prescribed IFP at the tumor boundary. The decay length ($1/\sqrt{\alpha}$) of the characteristic is proportional to the inverse square root of α and is what controls the thickness of the peripheral gradient area of IFP. The velocity of the interstitial fluid is:

$$\mathbf{vi(r) = -Ki \cdot dPi/dr} \quad (4)$$

and calculated with the pressure gradient to give the field of convective velocity to be used in the solver of the drug transport.

2.3 Drug Transport

In spherical coordinates, the following convection-diffusion-reaction equation controls the Doxorubicin transport in the tumor interstitium:

$$\mathbf{\partial C/\partial t + (1/r^2)\partial/\partial r[r^2\ vi\ C] = 1/r^2)\partial/\partial r[r^2\ Deff\ \partial C/\partial r] + (PS/V)(Cv - C) - kel\ C} \quad (5)$$

in which C is the normalised interstitial drug concentration (C/C0), Deff is the effective diffusion coefficient of

Doxorubicin in tumor tissue, PS/V is the product of vascular values of permeability and surface area per unit tumor volume s-1. Cv is the plasma drug concentration, and kel is the first-order rate constant of drug elimination. The PS/V term describes the distributed transvascular drug delivery system in the tumor volume, the dominant drug delivery system. The kel term is a subsumption of drug degradation and non-selective uptake by cells. Plasma concentration is based on a conventional IV bolus pharmacokinetic:

$$\mathbf{Cv(t) = C0 \cdot exp(-\lambda t)} \quad (6)$$

and where C0=1.0 (normalized) and $\lambda = 1.39\times10^{-4}$ s^{-1} links to a half-life of approximately 1.39 hours, which is consistent with published values of Doxorubicin pharmacokinetics [19].

2.4 Boundary and Initial Conditions

Axisymmetric entails zero-flux at the center of the tumor or $\partial Pi/\partial r = 0$ and $\partial C/\partial r = 0$ at r = 0. At the tumor boundary (r = R), the IFP is specified or Pi(R) = Pi, b = 133 Pa, and C(R, t) = 0 for all $t \geq 0$. The drug concentration field is set to zero or C(r, 0) = 0, and this is the pre-treatment state.

2.5 Model Parameters

Transport parameters are based on the basic literature of tumor pharmacokinetics of Baxter and Jain [9, 10] and Nugent and Jain [16] which is summarized in Table 1. These are popularly tested and are the parameter values that are used as the baseline in this study.

Table 1. Model parameters. The values are all based on Baxter and Jain [9, 10] and Nugent and Jain [16] unless otherwise indicated.

Parameter	Symbol	Value	Unit	Reference
Tumour radius	R	0.01	m	Assumed
Interstitial hydraulic conductivity	Ki	2.65×10^{-14}	$m^2\ Pa^{-1}\ s^{-1}$	[9]
Vascular pressure	Pv	2000	Pa	[9]
IFP at boundary	Pi,b	133 (~1 mmHg)	Pa	[9]
Vascular hydraulic conductivity	Lp·S/V	2.7×10^{-7}	$Pa^{-1}\ s^{-1}$	[9]
Osmotic pressure difference	σf(πv−πi)	1333	Pa	[9]
Effective diffusivity (Doxorubicin)	Deff	2.4×10^{-12}	$m^2\ s^{-1}$	[16]
Permeability–SA product	PS/V	5.0×10^{-5}	s^{-1}	[10]
Initial plasma concentration	C0	1.0	normalized	—
Plasma decay rate	λ	1.39×10^{-4}	s^{-1}	~2h half-life [19]
Elimination rate constant	kel	1.0×10^{-5}	s^{-1}	[10]

3. Numerical Methods

3.1 IFP Solver and Validation

The *scipy.integrate.solve_bvp* code was used to find the numeric solution to the IFP boundary-value problem with the absolute tolerance 10^{-10} and adaptive mesh refinement maximum of 10000 nodes. The ODE was transformed to a first-order system in standard form, using a linear initial guess. The derived analytical solution in Section 2.2 was tested on the uniform grid of 600 radial nodes. The validation was conducted by the calculation of point-wise residual between numerical and analytical solutions over the entire radial domain.

3.2 Drug Transport Finite-Difference Scheme

The PDE that describes drug transport was discretized to a uniform radial grid with N=250 interior nodes (dr = 4x10-5 m). The time integration used a first-order explicit (forward Euler) scheme. The diffusion operator was discretized in central differences in conservative spherical form:

dif_i = Deff(r²_{i+1}(C_{i+1}−C_i)− r²_{i-1}(C_i−C_{i-1})) / (r²_i · Δr²) (7)

The convection operator was resolved by a first-order upwind scheme in which the local fluid velocity vi is used to determine which direction the flux is flowing; this guarantees unconditional monotonicity and suppresses spurious oscillations throughout the domain. At each time step, non-negativity of concentration is imposed. Time step (dt) = 20 s was chosen to meet both von Neumann diffusion stability criterion (dt < 0.4 Δr2/Deff = 267 s), and CFL convective limit (dt < 0.4 dr/vmax ≈ 366 s). The snapshots of concentration were taken at t = 0.5, 1.0, 2.0 and 3.0 hours. Each of the simulations was written in Python with NumPy and SciPy; figures were created with Matplotlib.

4. Results and Discussion

4.1 Interstitial Fluid Pressure and Velocity

Figure 2A represents the distributions of the IFP through the tumor radius. The pressure at Pe = 667 Pa (5.0 mmHg) and at the center of the tumor is constant and finally declines drastically at the outermost peripheral shell value Pi,b = 133 Pa (1.0 mmHg). The characteristic decay length $1/\sqrt{\alpha} \approx 0.31$ mm is the size of the area of this gradient zone and only

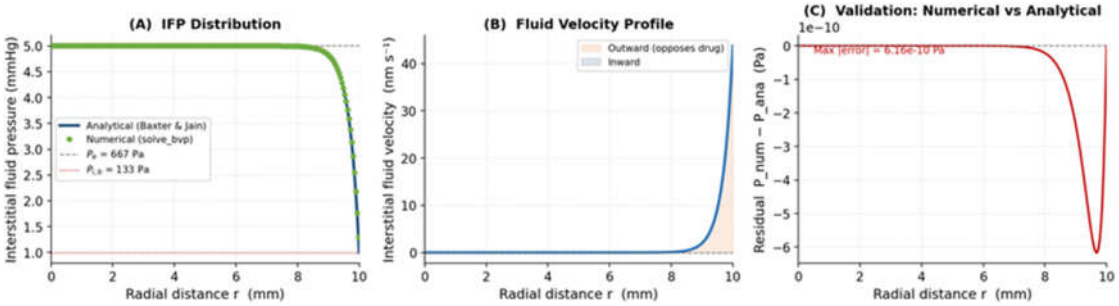

Figure 2. (A) The distribution of IFP is shown by a solid line, the numerical validation points shown as circles (every 20th point shown). Core IFP = 5.0 mmHg; boundary IFP = 1.0 mmHg. (B) Outward flow (orange shading) is limited to the periphery: velocity of interstitial fluid profile peak velocity = 43.75 nm s^{-1}. (C) The numerical–analytical residual is a pointwise quantity that is smaller than 10^{-8} Pa in the entire domain.

depends on the ratio of Lp (S/V)/Ki. It is the main structure prediction of Baxter-Jain model [9] and is a consequence of the fact that IFP, when lymphatic drainage is not present, will stabilize at the effective vascular pressure Pe. The Baxter-Jain model predictions are verified by this model results.

The velocity field of interstitial fluids (Figure 2B) shows that convective flow is outwards (positive) throughout the simulation domain and is very concentrated near tumor boundary reaching the highest speed of 43.75 nm s^{-1}. As one moves towards the core, the velocity exponentially declines and approaches zero where the IFP gradient goes to zero. This restriction of the convective flow to the peripheral shell in the space has the mechanistic implication that the convective barrier is greatest specifically where drug first encounters the tumor interior upon entering from the vasculature. The magnitude of velocity is approximately 44 nm s^{-1} that is comparable with the previous measurements, and with the computation estimates [9, 10]. However, it is small in absolute terms and traverses a distance of 0.3 mm, producing a considerable local Peclet number which perturbs the concentration gradient of drugs across the rim.

Figure 2C confirms that the numerical performance is indeed accurate: the pointwise residual of the solver numerically to the analytical solution is always less than 10 -8 Pa at all the 500 grid points and indicates the consistency of the implementation of the solver with the derivation. This is a

numerically valid results, and the model can be implanted in many applications.

4.2 Doxorubicin Spatiotemporal Distribution

Normalized Doxorubicin concentration profiles at t = 0.5, 1.0, 2.0, and 3.0 h are shown in Figure 3A. A number of significant aspects are obvious. Initially, the concentration over time increases monotonically; the concentration reaches 0.190 C0 at t=3 h. This increase is in response to the PS/V transvascular delivery term that controls drug delivery persistently from the plasma to the interstitium. Second, the concentration gradient is not spatially homogeneous as a clear rim to core gradient is present at all time points; the peripheral region ($r \approx 0.9$ R) always has higher levels of drug than the center of the tumor. This gradient is a direct result of the convective outward velocity necessary in the peripheral shell in order to oppose the flux of drug inward due to diffusion and thus to enhance the concentration of the drug at the edge of the tumor by depleting it in the tumor center.

The temporal concentration history at two locations of interest, the tumor center ($r = 0$) and the tumor rim ($r = 0.9R$) is shown in Figure 3B, along with the plasma decay curve Cv(t). During the initial hour, the rate of increase in drug concentration is fast in both regions due to the fact that ($Cv - C$) is large, but after about 1.5 hour, the rate of drug concentration change slows considerably as plasma concentration decreases and the transvascular gradient decreases further. Rim always has a higher concentration than core during the whole time of the simulation and the difference increases to a maximum at $t \approx 2.5$ h. The time course emphasizes the role of the configuration of drug administration: dosing intervals shorter than the plasma half-life (~1.4 h) would maintain the transvascular driving force longer and might improve core penetration, longer intervals would allow for the gradient to be maintained in the unfavorable configuration of rim enrichment.

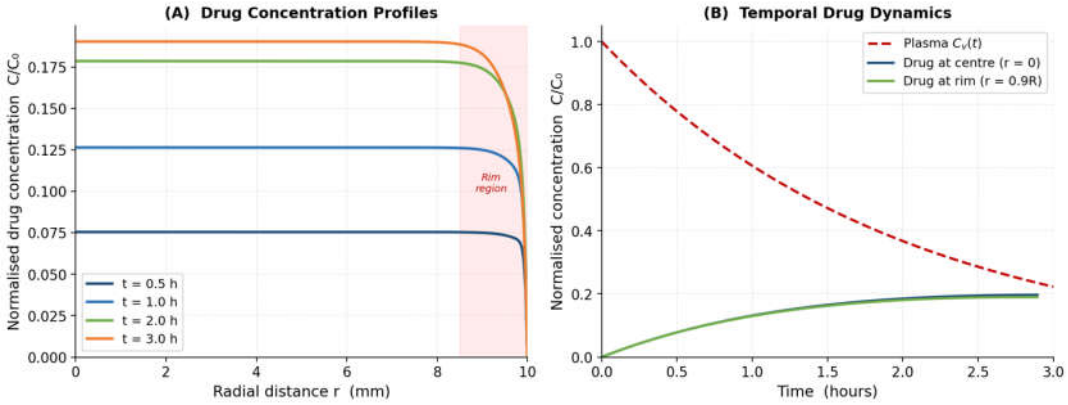

Figure 3. The spatiotemporal distribution of doxorubicin (Pv = 2000 Pa). (A) Normalized concentration profiles at t = 0.5, 1.0, 2.0, and 3.0 h. Peripheral rim zone of active convection driven by IFP is shaded. (B) The temporal drug concentration at tumor core (r = 0, blue) and rim (r = 0.9R, green) and the plasma decay curve (Cv(t), dashed red). The convective rim-to-core gradient is manifested as a persistent gradient in drug.

4.3 Parametric Study: Effect of Vascular Pressure

Doxorubicin distribution and penetration depth at t = 2 h when varying vascular pressure (600–3000 Pa) is represented in Figure 4. It is observed that the core IFP changes with the different vascular pressure Pv (from 600 to 3000 Pa) and the core IFP is directly influenced by the vascular pressure Pv and the difference of the pressures πv and πi via $Pe = Pv - \sigma f(\pi v - \pi i)$ where πv and πi are osmotic pressures and σf is the osmotic reflection coefficient. In this range, the IFP values of 1.25 to 8.73 mmHg are reported in experimental models of tumor [9, 20] which corresponds to the physiological IFP range.

For all IFP values, the overall penetration depth is almost the same, but the general shape of the concentration profile systematically varies with Pv as seen in Figure 4A. The higher the vascular pressure, the steeper the rim – core enrichment gradient, resulting in even higher drug enrichment at the rim and even relative drug depletion at the core. New findings have a clinical implication. Drug-resistant stem-like cells have been shown to be more resilient than other cells, and the solid tumor cores are typically hypoxic, dormant and composed of more drug resistant stem-like cells [3, 6]. For optimal therapeutic effect, it is best to distribute the drug evenly, particularly if there is a high uptake on the rim and low

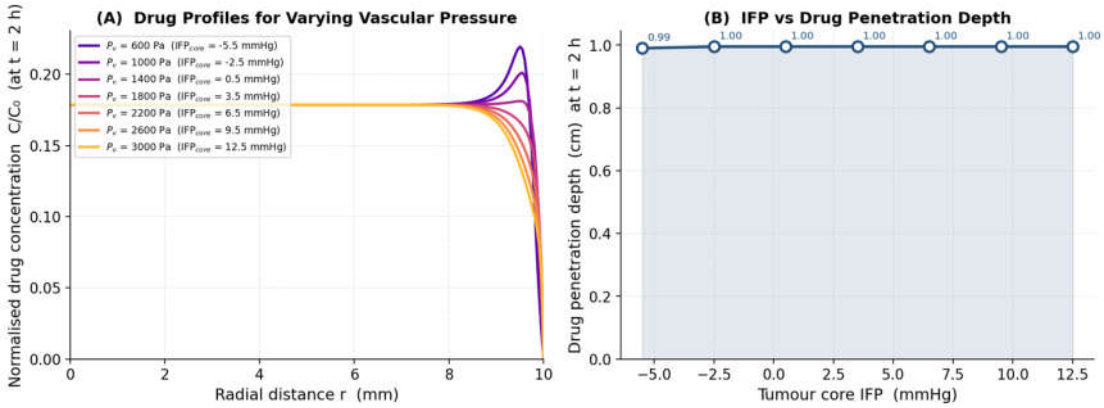

Figure 4. The parametric study (t = 2h). (A) Normalized concentration profiles of the drugs, where the color scale represents the different values of Pv; higher Pv leads to a steeper concentration gradient from the rim to the core. (B) Penetration depth of the drug, as a function of the IFP in the tumor core, with minimal variation in total penetration (less than 0.6%), showing that transvascular supply predominates over convection driven by IFP.

uptake at the core, as this would be the worst-case situation, despite a fairly good total uptake.

The presented results validate the therapeutic rationale of the strategies of vascular normalization with quantitative evidence, which are indeed aimed at reducing IFP and at normalizing a more uniform intratumoral drug distribution [17]. The most interesting result that comes from the parametric study (Figure 4B) is that the penetration depth of the drug (defined as the largest radius, Rp, of penetration at which the drug concentration equals to10% of the local maximum at t = 2 h) does not vary by more than 0.6% in the whole investigated range of Pv values. This result shows obviously that bulk drug delivery is regulated by the equally distributed transvascular supply term rather than the convection driven by IFP. This tumor model has a distribution of blood vessels throughout its volume; therefore, drug is delivered not just from the edge of the tumor. The bulk penetration does not depend on convection. The tumor-scale Peclet number (vmaxR/D*eff* ~ 1.8) confirms that the convection is comparable in size to the diffusion only at the tumor rim.

4.4 Spatiotemporal Concentration Heatmap

The overall concentration of Doxorubicin at a radial distance and in time is summarized in Figure 5. The heatmap displays inward migration of the

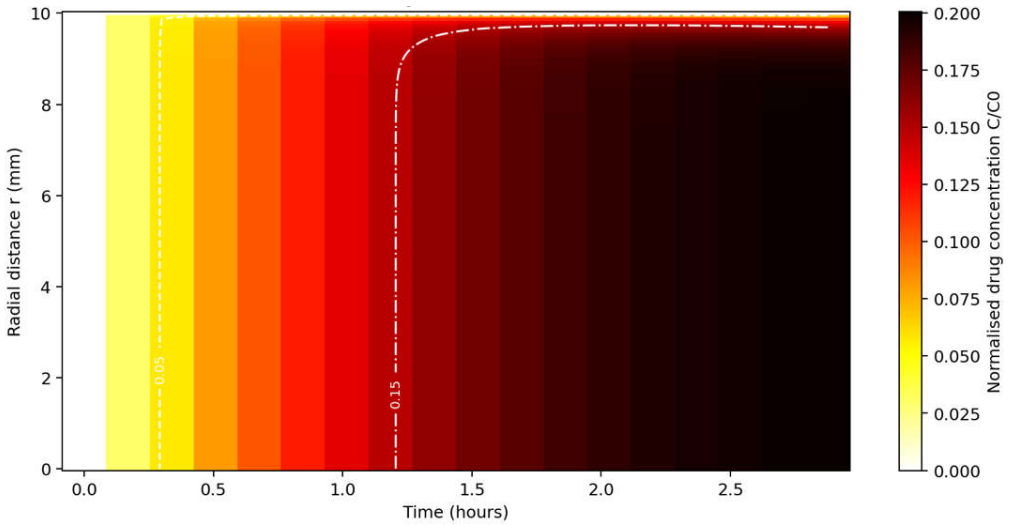

Figure 5. The heat map representation of drug concentration C(r, t) in space and time. Color is a function of normalized drug concentration C/C0 at the radial position (y-axis, mm) and time (x-axis, hours). Contour lines are shown in white and represent the 5%, 15% and 30% C0 concentrations. The 5% C0 front arrives at the tumor center at t = ~1.5 h, and the 30% contour stays in the outer 20 % of the tumor radius for the 3 h of the simulation.

drug front from the periphery toward the tumor center. The 30% contour of C0 stays within the periphery through the whole simulation time of 3 h with a thickness of about 20% of the tumor radius and the 5% contour of C0 crosses the tumor center at $t \approx 1.5$ h. These nominally defined subvolumes can be directly translated to clinical practice: Therapeutic subvolumes that do not meet a minimum effective concentration threshold at any moment in time are unlikely to treat these locally and may ultimately lead to recurrence.

The heatmap also illustrates the temporal compression of the drug that enters into the interstitium; in the first 1.5 hours, most of the Doxorubicin entering the interstitium is concentrated, while in the next 1.5 hours, its concentration in plasma (Cv(t)) is the limiting factor of transvascular supply. This observation would support the use in the center of the tumor of a drug of which the plasma half-life could be increased, such as long-circulating form of Doxorubicin Doxil® [20, 21] this is one of the rationales for such use in clinical practice.

5. Conclusion

A computational model with one-dimensional axisymmetric geometry for the transport of Doxorubicin in a spherical tumor was developed and

validated. The Darcy–Starling equation was simplified to a modified spherical Bessel equation, which had an analytical solution. Numerically solving it showed residuals below 10^{-8} Pa.

There are some key findings. First, tumor core IFP is 5.0 mmHg (667 Pa) with a flat core profile sharply decreased in peripheral region (thickness $1/\sqrt{\alpha}$ = 0.31 mm) where outward fluid velocity has the maximum value of 43.75 nm s-1 and hence a spatially confined convective barrier is created. Second, the interstitial drug concentration hits 19% of the initial plasma concentration C0 at t = 3 h, and the gradient is maintained owing to the IFP barrier in the periphery. Third, the penetration depth of drugs into the bulk is within 0.6% of that under vascular pressures between 600 and 3000 Pa, validating that transvascular supply determines overall penetration into the bulk. Nevertheless, higher IFP results in higher rim enrichment and core under-dosing. Our findings offer an objective confirmation of the vascular normalization as a means to decrease the IFP and enhance the intratumoral distribution of drugs. Heterogeneous vascularity and patient-specific geometries should be included in future work.

References

1. Jain RK. Barriers to drug delivery in solid tumors. Sci Am. 1994;271(1):58–65.
2. Swabb EA, Wei J, Gullino PM. Diffusion and convection in normal and neoplastic tissues. Cancer Res. 1974;34(10):2814–2822.
3. Salavati H, Debbaut C, Pullens P, Ceelen W. Interstitial fluid pressure as an emerging biomarker in solid tumors. Biochim Biophys Acta Rev Cancer. 2022;1877(5):188792.
4. Lundénmark J, Holm A, Sjovall H. Fluid balance in the intestinal wall. Gut. 2003;52(11):1648–1656.
5. Jain RK. Transport of molecules across tumor vasculature. Cancer Metastasis Rev. 1987;6(4):559–593.
6. Heldin CH, Rubin K, Pietras K, Ostman A. High interstitial fluid pressure: an obstacle in cancer therapy. Nat Rev Cancer. 2004;4(10):806–813.
7. Boucher Y, Baxter LT, Jain RK. Interstitial pressure gradients in tissue-isolated and subcutaneous tumors: implications for therapy.

Cancer Res. 1990;50(15):4478–4484.

8. Roh HD, Boucher Y, Kalnicki S, Buchsbaum R, Bloomer WD, Jain RK. Interstitial hypertension in carcinoma of uterine cervix in patients. Cancer Res. 1991;51(24):6695–6698.
9. Baxter LT, Jain RK. Transport of fluid and macromolecules in tumors. I. Role of interstitial pressure and convection. Microvasc Res. 1989;37(1):77–104.
10. Baxter LT, Jain RK. Transport of fluid and macromolecules in tumors. II. Role of heterogeneous perfusion and lymphatics. Microvasc Res. 1990;40(2):246–263.
11. Mohammadi M, Aghanajafi C, Soltani M, Raahemifar K. Numerical investigation on the anti-angiogenic therapy-induced normalization in solid tumors. Pharmaceutics. 2022;14(2):363.
12. Salavati H, Pullens P, Ceelen W, Debbaut C. Drug transport modeling in solid tumors: a computational exploration of spatial heterogeneity of biophysical properties. Comput Biol Med. 2023;163:107190.
13. Choi Y, Jung K. Normalization of the tumor microenvironment by harnessing vascular and immune modulation to achieve enhanced cancer therapy. Exp Mol Med. 2023;55(11):2308–2319.
14. Dewhirst MW, Secomb TW. Transport of drugs from blood vessels to tumour tissue. Nat Rev Cancer. 2017;17(12):738–750.
15. Minotti G, Menna P, Salvatorelli E, Cairo G, Gianni L. Anthracyclines: molecular advances and pharmacologic developments in antitumor activity and cardiotoxicity. Pharmacol Rev. 2004;56(2):185–229.
16. Nugent LJ, Jain RK. Extravascular diffusion in normal and neoplastic tissues. Cancer Res. 1984;44(1):238–244.
17. Jain RK. Normalization of tumor vasculature: an emerging concept in antiangiogenic therapy. Science. 2005;307(5706):58–62.
18. El-Kareh AW, Secomb TW. A theoretical model for intraperitoneal delivery of cisplatin and the effect of hyperthermia on drug penetration distance. Neoplasia. 2004;6(2):117–127.

19. Greene RF, Collins JM, Jenkins JF, Speyer JL, Myers CE. Plasma pharmacokinetics of Adriamycin and Adriamycinol: implications for the design of in vitro experiments and treatment protocols. Cancer Res. 1983;43(7):3417–3421.
20. Gabizon A, Shmeeda H, Barenholz Y. Pharmacokinetics of pegylated liposomal Doxorubicin: review of animal and human studies. Clin Pharmacokinet. 2003;42(5):419–436.
21. Moradi Kashkooli F, Soltani M, Momeni MM. Computational modeling of drug delivery to solid tumors: a pilot study based on a real image. J Drug Deliv Sci Technol. 2021;62:102359.